6808 *Macromolecules* **2009**, *42*, 6808–6815
DOI: 10.1021/ma901073y

Macromolecules
ARTICLE

Order−Disorder Transitions in Block Copolymer Electrolytes at Equilibrium with Humid Air

Moon Jeong Park[†,‡] **and Nitash P. Balsara***[,†,‡,§]

[†]*Department of Chemical Engineering, University of California, Berkeley, California 94720,* [‡]*Materials Sciences Division and* [§]*Environmental Energy Technologies Division, Lawrence Berkeley National Laboratory, University of California, Berkeley, California 94720*

Andrew Jackson

NIST Center for Neutron Research, National Institute of Standards and Technology, Gaithersburg, Maryland 20899, and Department of Materials Science and Engineering, University of Maryland, College Park, Maryland 20742

Received May 16, 2009

ABSTRACT: The effect of sulfonation level and domain size of hydrophilic channels on humidity-induced phase transitions in poly(styrenesulfonate−methylbutylene) (PSS−PMB) block copolymers was studied as a function of the relative humidity (RH) and temperature of the surrounding air by a combination of water uptake measurements and in situ small-angle neutron scattering. The equality of the chemical potential of water in the gas and polymer phases was exploited to determine the change in the partial molar entropy of water at order−disorder transitions. PSS−PMB samples with 5 nm domain spacing exhibited a disorder-to-order transition with increasing temperature at fixed RH, while the PSS−PMB samples with 7 nm domain spacing exhibited an order-to-disorder transition with increasing temperature at fixed RH. There is evidence to suggest that the disorder-to-order transition is driven by an increase in the partial molar entropy of the water molecules, while the order-to-disorder transition is driven by more familiar driving forces wherein entropic contributions stabilize the disordered phase.

Introduction

The partial molar entropy of components in polymer mixtures is a thermodynamic function of fundamental importance. The major breakthrough provided by the Flory−Huggins theory (FHT) was an expression for the partial molar entropy of homogeneous mixtures containing polymer chains.[1−3] This led to a quantitative understanding of macrophase separation in polymer blends. Similarly, the major breakthrough provided by self-consistent-field theory (SCFT) and the random phase approximation (RPA) was the ability to compute the partial molar entropy of individual components in microphase-separated systems wherein chain conformations are altered by the effective fields created by the microphases.[4−8] This led to a quantitative understanding of order−disorder transitions in block copolymers[6] and more complex multicomponent blends.[9−12] A convenient feature common to all of these theories—FHT, RPA, and SCFT—is that the entropic contributions can be calculated from molecular structure, which can be determined independently. The only adjustable parameter in these theories is χ_{ij}, the Flory−Huggins interaction parameter between components i and j in the mixture, which is related to internal energy contributions to the free energy.[1,13]

On the experimental side, one seldom measures partial molar entropy directly. The traditional approach has been to assume the applicability of either FHT, RPA, or SCFT and determine χ_{ij} by fitting experimental observations to the predictions of these theories. In theory, χ_{ij} should be proportional to $1/T$ and P (T and P are temperature and pressure, respectively) but independent of all other parameters such as component molecular weight, blend composition, and microphase-separated morphology. In virtually all cases, it is found that this is not true.[14] Fitting χ_{ij} vs $1/T$ data generally leads to large intercepts, and the magnitude of this intercept is often referred to as "entropic" contributions to χ. Similar problems arise when the measured χ_{ij} is found to depend on chain length[15] and composition.[16] There is clearly a need for developing methods for determining the partial molar entropy of components directly, i.e., without reference to theories such as FHT, RPA, and SCFT. This is especially true for mixtures of more complex components such as polyelectrolytes and water where the applicability of the above-mentioned theories is questionable.[17]

In a recent paper[18] we demonstrated that the change in the partial molar entropy of water in a block copolymer at an order−disorder transition (ODT), Δs_w, can be determined directly by measuring the ODT of the mixture in equilibrium with humid air. This approach, which is built on the assumption that the ODT is a first-order phase transition, exploits the fact that the chemical potential of a component in the gaseous phase, which is easy to predict,[19] is equal to that of the same component in the more complex phase such as a microphase-separated block copolymer electrolyte where predictions are more difficult. The proposed approach is perfectly general and can be applied to any volatile component (e.g., organic solvents) in contact with a block copolymer.

This paper is part of a series on the thermodynamics and phase behavior of poly(styrenesulfonate−methylbutylene) (PSS−PMB) copolymers in the presence of humid air.[18,20,21] In ref 20 we

*Corresponding author.

 Published on Web 07/02/2009

demonstrated that the water content of PSS−PMB membranes in contact with air at a fixed humidity increased with increasing temperature if the width of the PSS phase was below 6 nm. This was found to be true over a wide range of water concentration (RH of the air was varied from 50 to 98%) and temperatures (ranging from 25 to 90 °C). This resulted in a significant increase in proton conductivity within the membrane with increasing temperature. This "antidrying" property may lead to more efficient high-temperature fuel cells. In subsequent papers we explored the nature of microphase separation in dry PSS−PMB block copolymers as a function of temperature[21] and the alignment of the microphases at the polymer/humid air interface.[22] We demonstrated remarkably rich morphologies of lamellae, gyroid, hexagonally perforated lamellae, and hexagonally packed cylinders in nearly symmetric PSS−PMBs wherein the volume fraction of the PSS phase lies between 0.45 and 0.5. In this range of compositions, only lamellar phases are seen in uncharged block copolymers. It is therefore clear that self-assembly of sulfonated block copolymers is radically different from that of uncharged block copolymers. The purpose of this work, which follows ref 18 where the technique for measuring Δs_w was developed, was to measure Δs_w in a series of PSS−PMB copolymers and to study its effect on the phase behavior of PSS−PMB/water mixtures.

Experimental Section

Polymer Synthesis and Characterization. Polystyrene−polyisoprene block copolymers with polydispersity index of 1.03 were synthesized and characterized using methods described in ref 21. Selective hydrogenation of the polyisoprene block was conducted in the presence of a homogeneous Ni−Al catalyst with cyclohexane as the solvent, using a 2 L Parr batch reactor at 83 °C and 420 psi, following procedures given in ref 23. The hydrogenated block copolymers are referred to as poly(styrene−methylbutylene) (PS−PMB) copolymers. The number-averaged molecular weights of the blocks of the PS−PMB copolymers are $M_{n,PS} = 1.4$ kg/mol, $M_{n,PMB} = 1.4$ kg/mol and $M_{n,PS} = 2.5$ kg/mol, $M_{n,PMB} = 2.6$ kg/mol. We use the terms P1 and P3 to refer to these polymers where 1 and 3 are the nominal molecular weights of each of the blocks in kg/mol. The PS blocks of the PS−PMB copolymer were then sulfonated using procedures described in ref 24. Samples with different degrees of sulfonation were prepared by controlling reaction time. Samples are labeled according to the sulfonation level (SL); for example, in P1(18), 18% of the styrene monomers in the PSS block were sulfonated.

In-Situ Small-Angle Neutron Scattering (In-Situ SANS). The in-situ SANS samples were prepared by solvent casting the polymer from THF solutions on 1 mm quartz windows. The sample thickness ranged from 110 to 150 μm, and a circular area with a diameter of 1.8 cm was exposed to the neutron beam. The samples were studied using the 30 m NG3 beamline at the National Institute of Standards and Technology (NIST) equipped with a sample holder wherein the humidity of the surrounding air and sample temperature were controlled.[25] Water from a well located within the sample chamber was used to humidify the air around the sample. In our experiments, the well was filled with either pure D_2O or pure H_2O. The uncertainty of the sample humidity and temperature for the NIST humidity sample chamber are ±1% RH and ±1 °C, respectively. The lowest RH limit and the highest temperature limit of the NIST environmental chamber are RH = 25% and $T = 80$ °C, respectively. Samples were equilibrated for at least 30 min before measurement. Separate transient measurements were conducted as a function of sample thickness to ensure that this equilibration time was adequate for the temperature and humidity steps used in our study. The raw data were converted to absolute coherent scattering intensity, I, as a function of scattering wave vector q ($q = 4\pi \sin(\theta/2)/\lambda$, where θ is the scattering angle and λ is the wavelength of the incident neutrons) after corrections for detector sensitivity, background, empty cell, and incoherent scattering were made, using standard procedures.[26] The wavelength of the incident neutron beam (λ) was 0.6 nm ($\Delta\lambda/\lambda = 0.10$), and sample-to-detector distances of 1.0, 3.0, and 12.0 m were used. This enabled access to scattering at q values in the range 0.03−5.9 nm^{-1}.

Water Uptake Measurements. Polymer films with thickness ranging from 100 to 150 μm were prepared by solvent casting from 10 wt % THF solutions. The films were dried at room temperature for 3 days under a N_2 blanket and under vacuum at 60 °C for 5 days. The dry weights of the membranes were obtained right after vacuum drying. The films were then exposed to humidified air in an ESPEC SH-241 humidity chamber. The increments of weight were measured using a Mettler balance with 0.01 mg accuracy. Samples were studied as a function of temperature ranging from 25 to 80 °C and RHs from 50 to 98%. The water uptake is calculated using the dry film as the basis:

$$\text{water uptake} = \frac{\text{weight of wet film} - \text{weight of dry film}}{\text{weight of dry film}} \times 100\% \quad (1)$$

The reported water uptake values are based on measurements from five independent samples. The standard deviation of the measurements was less than 5% of the averaged values.

Results and Discussion

The morphology of dry P1 and P3 copolymers as a function of SL and temperature was determined using methods outlined in

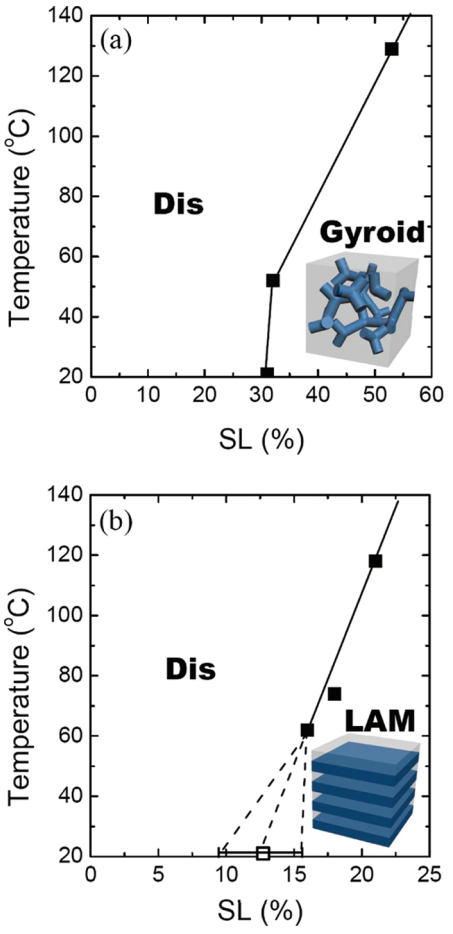

Figure 1. Phase diagrams of (a) P1 series and (b) P3 series in dry state on temperature versus sulfonation level (SL) plots. The dashed lines in (b) represent uncertainty of the phase boundary.

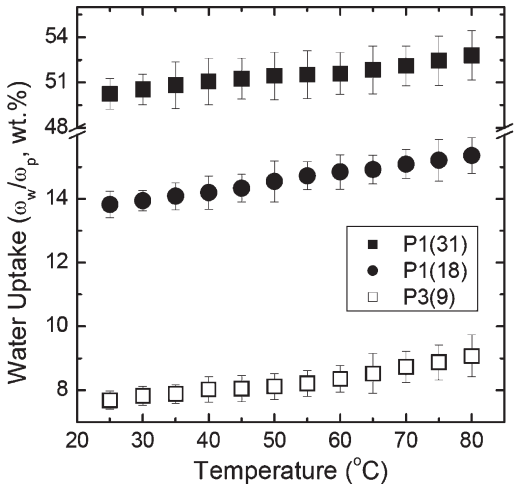

Figure 2. Water uptake, $\omega_w/\omega_p \times 100$ (%), where ω_w is the weight of water and ω_p is the weight of polymer, of P1(31), P1(18), and P3(9) at a fixed RH = 85% as a function of temperature. Error bars represent 1 standard deviation.

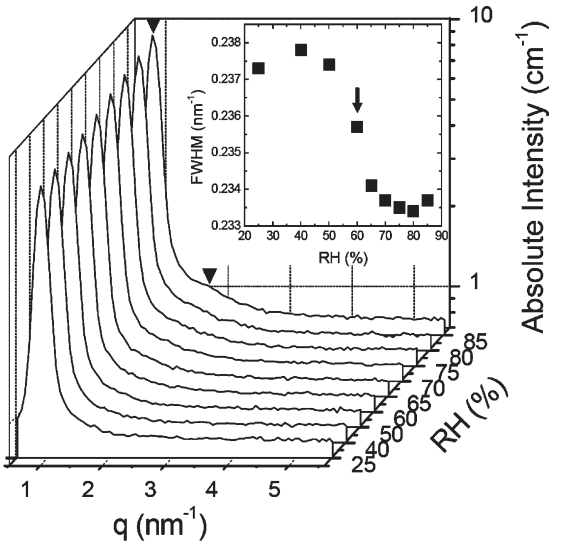

Figure 3. In-situ SANS intensity, I, versus scattering vector, q, of P3(9) at 25 °C as a function of RH with D_2O vapor. The presence of a second-order scattering peak at $q = 2q_{max}$ indicates the presence of a lamellar ordered phase at RH > 60%. Inset box clearly shows a discontinuous decrease in fwhm of the primary scattering peak at RH = 60%, indicating a humidity-induced disorder-to-order transition.

ref 21 (SAXS and electron microscopy), and the results are shown in Figures 1a and 1b, respectively. Increasing SL results in the stabilization of the ordered phase, which is consistent with previous results.[21] For P1 samples, P1(31) was disordered at room temperature while P1(32) was ordered and exhibited an ODT from gyroid to disorder at $T_{ODT} = 54 \pm 1$ °C. Obtaining samples with 31 and 32% SLs was fortuitous because the relationship between sulfonation reaction time and SLs appears to depend on many factors beyond our control. For P3 samples, P3(9) was disordered at room temperature while P3(16) was ordered and exhibited an ODT from lamellae to disorder at $T_{ODT} = 62 \pm 1$ °C. In this case, repeated attempts to synthesize sulfonated samples with SL values between 9 and 16% were unsuccessful. There is thus considerable uncertainty in the boundary between the lamellar and disordered phases in P3 at low SLs. The dashed lines in Figure 1b indicate the bounds for the boundary. The transition from disorder to order at room temperature of P3 occurs at SL = 12.5 ± 3.5%, which is substantially lower than that of P1 (compare Figures 1a and 1b). This is due to differences in chain length ($N = 99$ for P3 while $N = 54$ for P1; N is the number of monomer units based on a reference volume of 0.1 nm^3) and the strong increase of χ between PSS and PMB chains with increasing SL.[21]

In Figure 2, we show the water uptake data of P1(31), P1(18), and P3(9) as a function of increasing temperature at a fixed RH = 85%. The data are similar to those reported in ref 20 where data obtained from various PSS−PMB systems are reported. The concentrations of water in P1(31), P1(18), and P3(9) increase with increasing temperature of the surrounding air at fixed RH. This "antidrying" property is only obtained in PSS−PMB copolymers wherein the width of the hydrophilic phase is less than 6 nm.[20] The data in Figure 2 indicate the antidrying is a property of PSS−PMB copolymers at SLs as low as 9%.

The effect of the humidity and temperature of the surrounding air on the equilibrated structure of P3(9) is shown in Figure 3, where we show in-situ SANS profiles obtained from a 113 μm thick film exposed to a D_2O/air environment. At RH = 25% and $T = 25$ °C a broad primary peak at scattering vector $q_{max} = 0.89$ nm^{-1} indicates the presence of a disordered phase. A monotonic increase in $I(q_{max})$ with increasing RH is observed. When the RH is switched from 50 to 60%, we see a discontinuous decrease in the full width at half-maximum (fwhm) of the primary peak, as shown in the inset of Figure 3, and the emergence of an additional scattering shoulder at $q = 2q_{max}$. This indicates the presence of a lamellar phase at RH > 60%. Using the data in the inset of Figure 3, we conclude that the disorder-to-order transition (DOT) of P3(9) at 25 °C occurs at RH = 60 ± 5%.

In-situ SANS data from P3(9) obtained as a function of increasing temperature at a fixed RH = 85% are shown in Figure 4a. In this experiment D_2O was used to humidify the air surrounding the sample. Up to a temperature of 46 °C, we observed the presence of a sharp primary scattering peak at $q = q_{max}$ with a fwhm in the vicinity of 0.25 nm^{-1} (inset of Figure 4a). The presence of a second-order scattering peak at $q = 2q_{max}$ indicates the presence of a lamellar ordered phase in this temperature window. Increasing the sample temperature to 48 °C results in an abrupt increase in the fwhm of the peak (inset of Figure 4a), the disappearance of the second-order peak, and a discontinuous decrease in the intensity of the primary scattering peak (Figure 4a). These observations indicate the presence of an ODT at 48 °C and RH = 85%.

In-situ SANS data from P3(9) with H_2O in the humidified air, obtained as a function of increasing temperature at a fixed RH = 85%, are shown in Figure 4b. An abrupt increase in fwhm of primary SANS peak at 48 °C is taken as the signature of the ODT in PSS−PMB/H_2O mixtures (Figure 4b, inset). Since T_{ODT} in the presence of H_2O and D_2O are within experimental error (Figures 4a and 4b), we conclude that the effect of deuterium substitution on phase behavior of PSS−PMB/water mixtures is negligible.

In nearly all of the data published on scattering from block copolymers in the vicinity of the ODT [e.g., refs 27−29], the ODT is characterized by a change in the slope of the $1/I(q_{max})$ versus $1/T$ data. In addition, $1/I(q_{max})$ approaches zero as the ODT is approached from the disordered side due to a dramatic increase in the magnitude of concentration fluctuations.[4,6,30,31] The data obtained from PSS−PMB/D_2O mixtures differ dramatically from these expectations. This is made clear in Figure 4c (filled symbols) where we plot $1/I(q_{max})$ versus $1/T$ for the PSS−PMB/D_2O data set shown in Figure 4a. We see little change in $1/I(q_{max})$ as the ODT of PSS−PMB/D_2O mixtures is approached from the disordered side. In fact, $1/I(q_{max})$ increases slightly [i.e., $I(q_{max})$ decreases] as the ODT is approached from the disordered side. This unexpected result is due to two opposing tendencies. As temperature decreases, the magnitude of the concentration

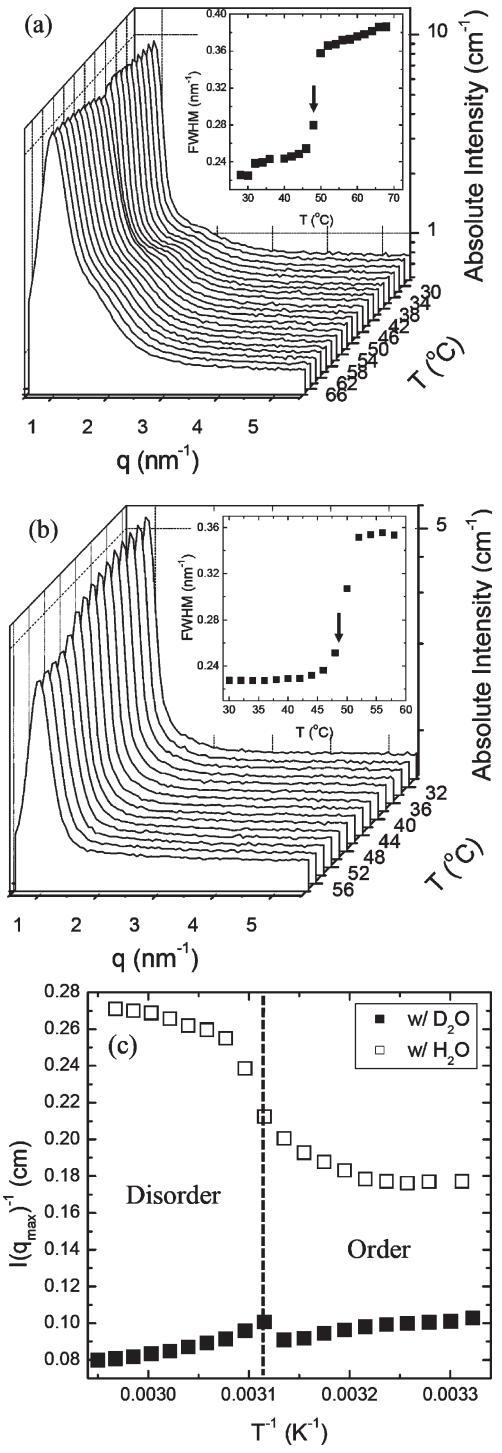

Figure 4. In-situ SANS intensity, I, versus scattering vector, q, of P3(9) as a function of temperature at RH = 85% (a) with D_2O vapor and (b) with H_2O vapor. Both results indicate a temperature-induced lamellar-to-disorder transition at 48 °C. Inset box clearly shows a discontinuous increase in fwhm of the primary scattering peak at T = 48 °C. (c) $1/I(q_{max})$ versus $1/T$ plots using SANS profiles in (a) and (b).

fluctuations increases as the ODT is approached from the disordered side, but the neutron scattering contrast between the PSS-rich and PMB-rich regions decreases due to the fact that the D_2O molecules associated primarily with the PSS-rich regions evaporate into the surrounding air (note that our system exhibits "antidrying"). This is confirmed by examining the unfilled data in Figure 4c, which were obtained from PSS−PMB/H_2O mixtures.

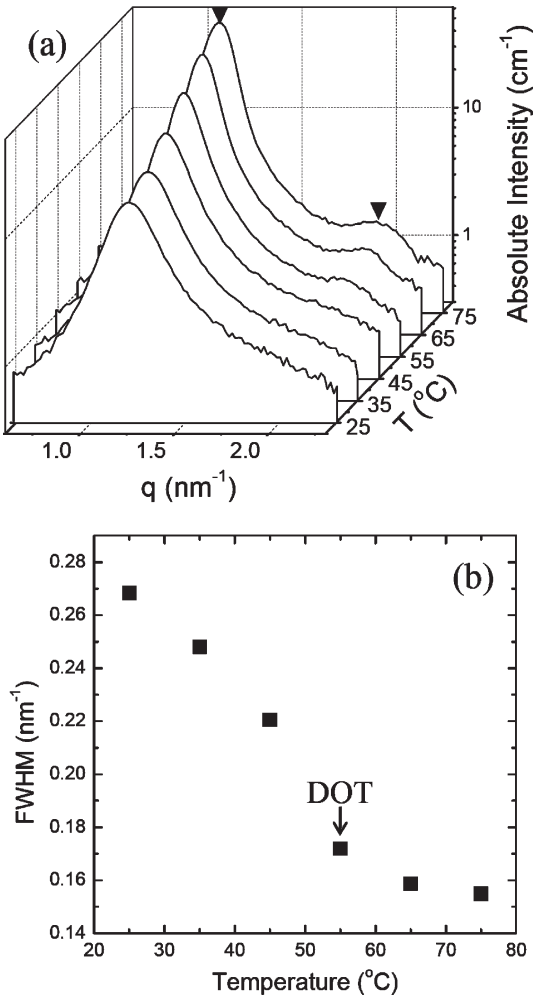

Figure 5. In-situ SANS data of P1(18) at RH = 85% as a function of temperature with D_2O vapor. (a) SANS intensity, I, versus scattering vector, q. The presence of a second-order scattering peak at $q = 2q_{max}$ indicates the presence of a lamellar ordered phase at T above 55 °C. (b) Full width at half-maximum (fwhm) of the SANS peaks versus temperature. A discontinuous decrease in fwhm of the primary scattering peak at T = 55 °C indicates a humidity-induced disorder-to-order transition.

Here we see the changes in the slope of the $1/I(q_{max})$ versus $1/T$ data in the vicinity of the ODT, as expected. It is clear that the nature of the concentration fluctuations in our system are more accurately reflected in the H_2O experiments than the D_2O experiments. However, the nature of the ordered phase is better studied in the D_2O experiments; note that the low contrast between the hydrophobic and hydrophilic domains in PSS−PMB/H_2O mixtures precluded observation of the second-order peak from the lamellar phase (Figure 4b). For completeness, the neutron scattering length density (SLD) of PS, PSS (SL = 100%), and PMB is 1.41×10^{-6}, 2.05×10^{-6}, and -0.31×10^{-6} Å^{-2}, respectively.

P3(9) was examined at several other values of RH and behavior similar to that reported in Figure 4 was also observed: T_{ODT} = 50 °C at RH = 70% and T_{ODT} = 44 °C at RH = 95%. At RH < 60%, P3(9) was disordered over the entire accessible T-window. In the disordered state, the SANS intensity of P3(9)/H_2O mixtures decreases monotonically with increasing temperature, which implies upper critical solution temperature (UCST) behavior. The phase behavior of dry P3 samples also indicates UCST behavior; i.e., ordered microphase-separated phases are seen at low temperatures while disordered homogeneous phases are seen at high temperatures. For brevity, we do not show these data

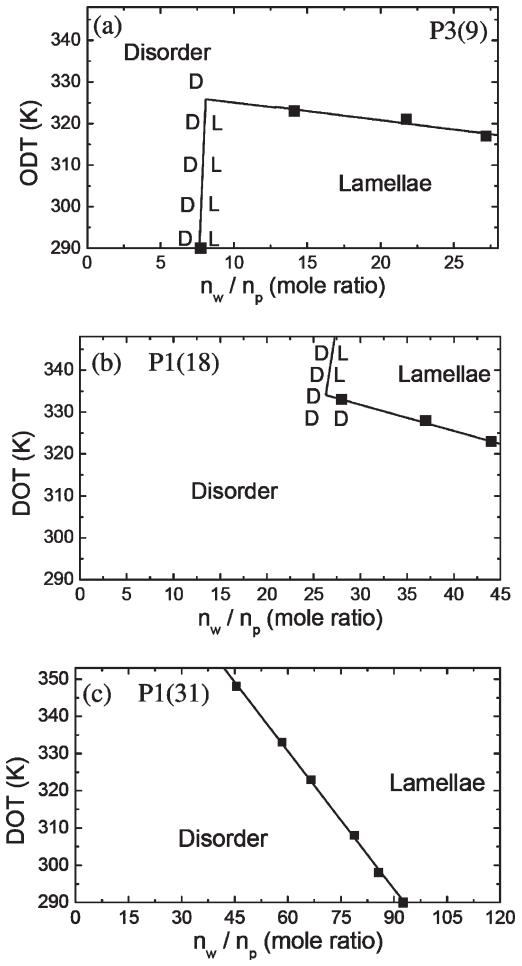

Figure 6. Phase behavior of P3(9), P1(18), and P1(31) on temperature (T) versus molar ratio of water to polymer in the membrane (n_w/n_p) plots. The n_w/n_p values were obtained from water uptake measurements. The letters D and L show the values of T and n_w/n_p near the phase boundary where the disordered and lamellar phases were obtained.

here. The thermodynamic properties of P3(9) under humid conditions are thus similar to those of P3 samples under dry conditions.

In-situ SANS data obtained from P1(18) in D_2O/air environment at RH = 85% as a function of increasing temperature are shown in Figure 5a. At low temperatures we obtain a broad scattering profile, indicating the presence of a disordered phase. Increasing the temperature to 55 °C results in an abrupt decrease in fwhm of the primary scattering peak (Figure 5b) and the appearance of a second-order scattering peak at $q = 2q_{max}$. It is clear that in spite of the similarities of P3(9) and P1(18) in the dry state (Figure 1) and water uptake characteristics (Figure 2), the behavior obtained in humid conditions is totally different. While P3(9) exhibits an ODT with increasing temperature, P1(18) exhibits a DOT with increasing temperature. The DOT temperature, T_{DOT}, of P1(18) was determined as 55 °C at RH = 85%. Similar phase behavior was observed at other RH values: T_{DOT} = 60 °C at RH = 75% and T_{DOT} = 50 °C at RH = 95%. P1(18) was disordered across the entire temperature window for RH < 65%.

The phase diagrams of P3(9), P1(18), and P1(31) in the presence of humid air are shown in parts a, b, and c of Figure 6, respectively, in plots of T versus n_w/n_p, where n_w and n_p represent moles of water and block copolymer, respectively, in the sample. The water uptake measurements were used to obtain the water concentration in the membrane (n_w/n_p). A nearly vertical line

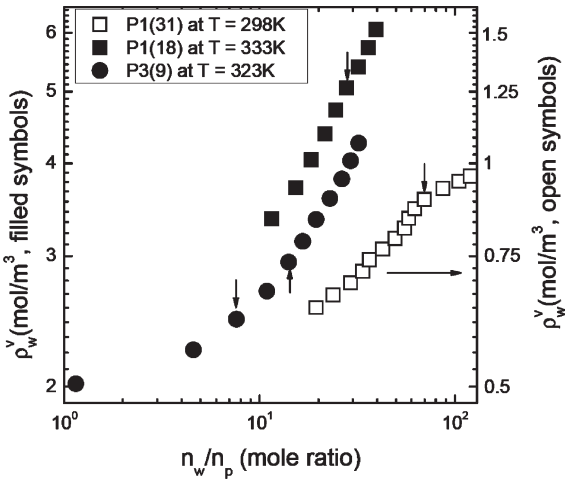

Figure 7. Molar concentration of water in the surrounding air (ρ_w^v, mol of water per m^3 of dry air) at different RH values versus n_w/n_p of P1(31) at 25 °C, P1(18) at 60 °C, and P3(9) at 50 °C. The DOTs of P1(31), P1(18), and P3(9) determined by in-situ SANS are indicated by an inverted arrow (↓) while the ODT of P3(9) is shown by an arrow (↑).

distinguishes between order and disorder in both P3(9) and P1(18) samples. However, the role of temperature is reversed in the two cases: increasing temperature stabilizes the disordered phase in P3(9) and the ordered phase in P1(18). For completeness, we also show the phase diagram of P1(31) using data presented in ref 18. In this case, increasing temperature stabilizes the ordered phase as was the case with P1(18). The nearly vertical division between order and disorder is not seen in this sample. Whether it is due to the limited temperature window of our experiments or an intrinsic difference between P1(18) and P1(31) is not clear at this juncture.

We use the thermodynamic framework introduced in ref 18 to analyze the phase behavior of PSS−PMB/water mixtures shown in Figure 6. The final result of that analysis, which was based on equating the chemical potential of water in the air and polymer phases, is

$$\frac{dT_t}{d(n_w/n_p)} = \frac{\Delta\left(\frac{\partial\mu_w}{\partial(n_w/n_p)}\right)_T}{\Delta s_w} = \frac{\frac{RT}{\rho_w^v}\Delta\left(\frac{\partial\rho_w^v}{\partial(n_w/n_p)}\right)_T}{\Delta s_w} \qquad (2)$$

where T_t is the phase transition temperature, s_w is partial molar entropy of water, ρ_w^v is the concentration of water vapor in the air (moles of water per unit volume of air), Δ refers to the difference between the quantity of interest in the ordered and disordered states, and μ_w is the chemical potential of the water in the block copolymer. The analysis assumes that the discontinuity of water concentration in the copolymer across the ODT is negligible, and the coexistence between ordered and disordered phases occurs over a narrow window. Our only justification for making these assumptions is that they are consistent with all of our experimental measurements conducted thus far (e.g., Figure 2).

The water uptake data (e.g., Figure 2) for P1(31), P1(18), and P3(9) were converted into plots of ρ_w^v versus n_w/n_p, and typical results thus obtained are shown in Figure 7. The inverted arrows (↓) in Figure 7 indicate the location of DOTs for the three systems while the arrow (↑) shows the ODT for P3(9). There is generally a subtle change in the water uptake in the ordered state relative to the disordered state. In the case of sample P3(9), we see an increase in the gradient of the ρ_w^v versus n_w/n_p data at the DOT. On the other hand, for sample P1(31), we see a decrease in the gradient of the ρ_w^v versus n_w/n_p data at the phase transition. Note that our thermodynamic analysis is based on slope differences of

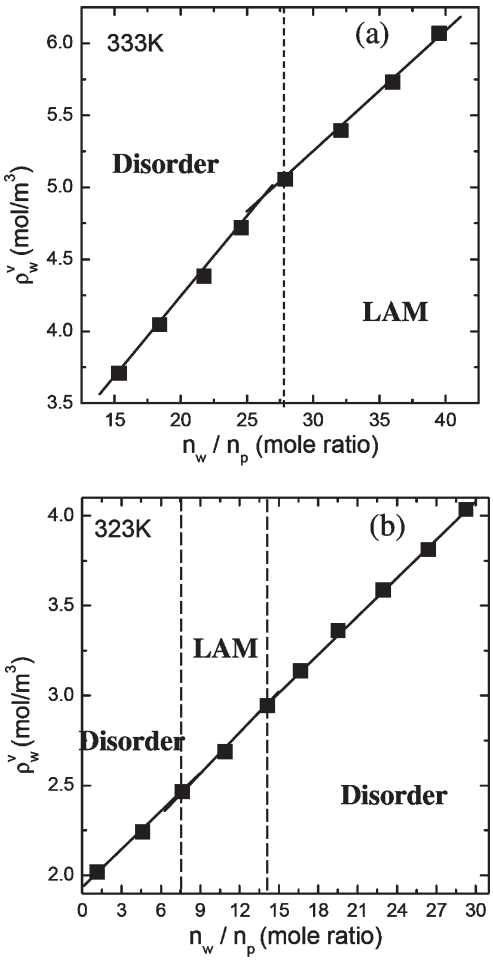

Figure 8. Molar concentration of water in the surrounding air (ρ_w^v, mol of water per m^3 of dry air) at different RH values versus n_w/n_p of (a) P1(18) at 60 °C and (b) P3(9) at 50 °C. Least-squares linear fits through the ρ_w^v versus n_w/n_p data obtained in the ordered and disordered states are used to calculate $\Delta[\partial\rho_w/\partial(n_w/n_p)]_{DOT}$.

linear−linear ρ_w^v versus n_w/n_p data (eq 2) while Figure 7 shows the data on a semilog plot.

It is clear from Figure 7 (and numerous other data sets obtained from PSS−PMB copolymers) that the dependence of ρ_w^v versus n_w/n_p is generally unremarkable. We find no evidence of dramatic changes in the dependence of ρ_w^v on n_w/n_p at ODT. We thus conclude on the basis of eq 2 that any dramatic changes in the slope of T_t versus n_w/n_p data must arise from dramatic changes in Δs_w. On the basis of eq 2, we also conclude that a vertical phase boundary in a T versus n_w/n_p plot (Figure 6) is obtained if Δs_w is zero (or nearly so) but $\Delta[\partial\rho_w^v/\partial(n_w/n_p)]_T$ is finite. We thus conclude from the data in Figure 7 that $\Delta s_w = 0$ at $n_w/n_p = 7.7$ for P3(9) and at $n_w/n_p = 26.5$ for P1(18). The finite slopes of the T_t versus n_w/n_p data at $7.7 < n_w/n_p < 27.2$ for P3(9), at $26.5 < n_w/n_p < 44$ for P1(18), and $46.5 < n_w/n_p < 92.5$ for P1(31) seen in Figure 6 indicate that Δs_w is finite in these regimes. The slopes of the phase boundaries in these regimes are -0.45 ± 0.41 K for P3(9), -0.62 ± 0.14 K for P1(18), and -1.23 ± 0.04 K for P1(31). All of the uncertainties listed here and in the paragraph below are based on the Student distribution with a confidence interval of 80%. In the discussion below, we study the implications of these phase boundaries.

Since the numerator of the last term in eq 2 can be obtained from water uptake measurements, the measured slopes of the T_t versus n_w/n_p phase boundaries in Figure 6 can be used to estimate Δs_w. In Figure 8 we show ρ_w^v versus n_w/n_p plots for P1(18) and P3(9). The lines in Figure 8 are least-squares linear fits through the ρ_w^v versus n_w/n_p data obtained in the ordered and disordered states. As noted above, there is only a subtle change in the water uptake characteristics at the DOT. The value of $\Delta[\partial\rho_w^v/\partial(n_w/n_p)]_{DOT}$ of P1(18) is $-(1.8 \pm 0.8) \times 10^{-2}$ mol/m^3 (Figure 8a), which in turn yields $\Delta s_w = 16.1 \pm 3.9$ J/(mol K) at 60 °C. The above method was used to calculate Δs_w at other DOT points of P1(18) yielding values of 18.4 at 55 °C and 11.5 at 50 °C. The average value of Δs_w for P1(18) is thus 15.3 ± 3.7 J/(mol K). Similarly, $\Delta s_w = 5.8 \pm 0.47$ J/(mol K) for P1(31).[18] For P3(9) $\Delta[\partial\rho_w^v/\partial(n_w/n_p)]_{DOT} = (3.6 \pm 0.5) \times 10^{-3}$ mol/m^3 (Figure 8b), which is an order of magnitude lower than that of P1(18). The small difference in slopes and the fact that T_t is insensitive to changes in n_w/n_p (Figure 6a) leads to considerable uncertainty in our analysis of the P3(9) data. We obtain $\Delta s_w = -11.4 \pm 10.5$ J/(mol K) for P3(9). We have only used one point to evaluate Δs_w (50 °C). At this temperature the ordered window is the widest, thereby enabling determination of the dependence of ρ_w^v on n_w/n_p with the greatest accuracy (see Figure 6a).

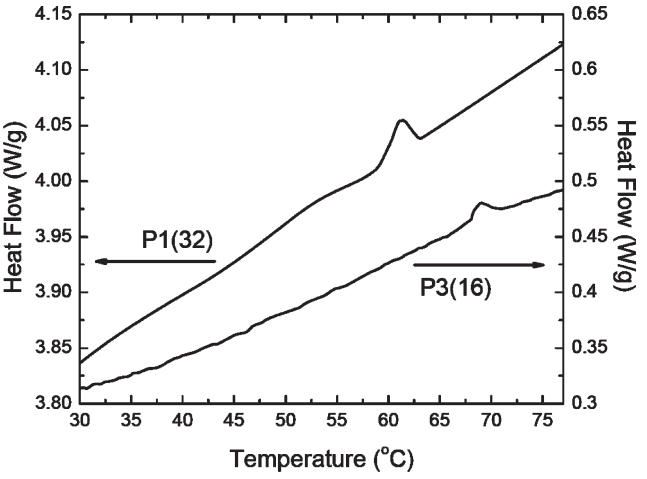

Figure 9. DSC trace obtained from P1(32) and P3(16) at a rate of 1 °C/min. The temperature dependencies of heat flow versus temperature are shown. The difference between the baselines of the two samples is due to background subtraction of DSC data.

Estimates of the partial molar entropy change of the polymer chains, Δs_p, were obtained from DSC experiments on P1(32) and P3(16). These are samples with SL values that are similar to those of the polymers of interest but with accessible ODTs in the dry state (Figure 1). Ideally, we would have liked to conduct DSC experiments on P1(31), P1(18), and P3(9) samples under controlled humidity, but we did not have access to such instrumentation. The DSC traces of dry P1(32) and P3(16) shown in Figure 9 indicate that the changes in molar enthalpy at the ODT of the samples, Δh_p, are −714 and −702 J/mol, respectively (the molecular weights of P1(32) and P3(16) are 3200 and 5400 g/mol). Δs_p, which is then equal to $\Delta h_p/T_{ODT}$, is −2.13 and −2.06 J/(mol K) for samples P1(32) and P3(16), respectively.

Consider a binary polymer blend of chains with equal numbers of monomers, N. The expression for ΔG, the Gibbs free energy change of mixing per unit volume, according to the Flory−Huggins theory, is

$$\frac{\Delta G v}{kT} = \frac{\phi_1 \ln \phi_1}{N} + \frac{(1-\phi_1)\ln(1-\phi_1)}{N} + \chi\phi_1(1-\phi_1) \qquad (3)$$

where ϕ_1 is the volume fraction of component 1 in the mixture, v is a reference volume, k is the Boltzmann constant, T is the absolute temperature, N is the number of repeat units per chain, where each repeat unit is assumed to have a volume equal to v, and χ is the Flory−Huggins interaction parameter based on the reference

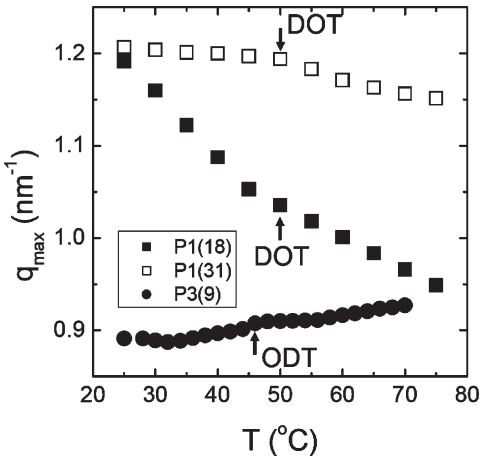

Figure 10. Dependence of q_{max} values on temperature at RH = 65% for P1(31) (open symbols) and at RH = 95% for P1(18) and P3(9) (filled symbols). T_{DOT} of P1(31) and P1(18) and T_{ODT} of P3(9), obtained from in-situ SANS, are indicated in the figure by arrows.

volume v. The first two terms of the right-hand side of eq 3 represent ΔS, the entropy change of mixing. The partial molar entropy change of mixing of polymer 1, $\Delta s_p = R \ln \phi_1$. For a critical mixture with $\phi_1 = 0.5$, setting $\Delta G = 0$, eq 3 gives $\ln \phi_1 = -\chi N/4$. For a mixture on the verge of phase separation, $\chi N = 2$, and $\Delta s_p/R = -\chi N/4 = -0.5$.

The purpose of the calculation given above is to present arguments indicating that for simple polymer systems in the vicinity of phase separation transitions $\Delta s_p/R$ is expected to be a negative number of order unity that is independent of the molecular weight of the chains. We note in passing that the partial molar entropy change of a polymer mixture at the critical point is zero, as is the case for all second-order phase transitions. The ODT in block copolymers is a weak first-order phase transition,[4,32−34] and we thus expect $\Delta s_p/R$ to be a negative number of order unity. In a private communication, G. H. Fredrickson suggested a method for estimating $\Delta s_p/R$ for a symmetric block copolymer at the ODT. He argued, based on his analysis in ref 33, that the free energy change at the ODT is 1.19 $(\chi N)^{1/3}$, of which $0.4(\chi N)^{1/3}$ can be attributed to chain stretching and the remainder to interfacial energy in units of kT per chain. This penalty, when balanced against the enthalpy of a fully mixed state ($\chi N/4$, identical to the polymer blend case described above), yields $\chi N = 10.4$ at the ODT. Assuming that Δs_p is dominated by the stretching contribution, Fredrickson obtained $\Delta s_p/R = -0.4(\chi N)^{1/3}$, which, at the ODT, yields $\Delta s_p/R = -0.88$. This value is similar to that obtained for the blend. Our experiments on P1(18) and P3(9), which indicate that $\Delta s_p/R$ is independent of molecular weight and approximately equal to −0.25, are qualitatively consistent with the theoretical arguments given above.

Lacking a more sophisticated model, we assume that the total molar entropy change in the humidified samples at the vicinity of ODTs and DOTs, $\Delta s_{total} = (n_w \Delta s_w + n_p \Delta s_p)/(n_w + n_p)$, where Δs_p is based on the results obtained from the dry samples and Δs_w is determined from our analysis based on eq 2. In the cases of P1(31) and P1(18), we obtain Δs_{total} to be 5.6 ± 0.5 and 14.7 ± 3.5 J/(mol K), respectively. It is clear an increase in the total entropy of the system is a major driving force for the humidity-induced order formation observed in P1(31) and P1(18). On the other hand, Δs_{total} for P3(9) is -10.8 ± 9.9 J/(mol K). In this case, entropic effects oppose order formation, as is typically the case.

In Figure 10 where we plot the temperature dependence of q_{max} of P3(9), P1(18), and P1(31) at RH values where accessible ODTs and DOTs were obtained. Sample P1(18) is particularly noteworthy as q_{max} decreases by 26% as temperature is increased from 25 to 75 °C. Such large changes in q_{max}, indicating substantial swelling of the lamellae with increasing temperature, are generally not observed in conventional block copolymers. This is also the sample with the largest positive Δs_w. Modest swelling with increasing temperature is observed in P1(31) where Δs_w is positive, but not as large. Modest deswelling with increasing temperature is observed in P3(9) where Δs_w is negative. The behavior of P3(9) is similar to that of dry conventional block copolymers in the vicinity of the ODT. It is evident that there is a complex relationship between overall water uptake, swelling or deswelling of the microphases, and the partial molar entropy of water in hydrated PSS−PMB systems.

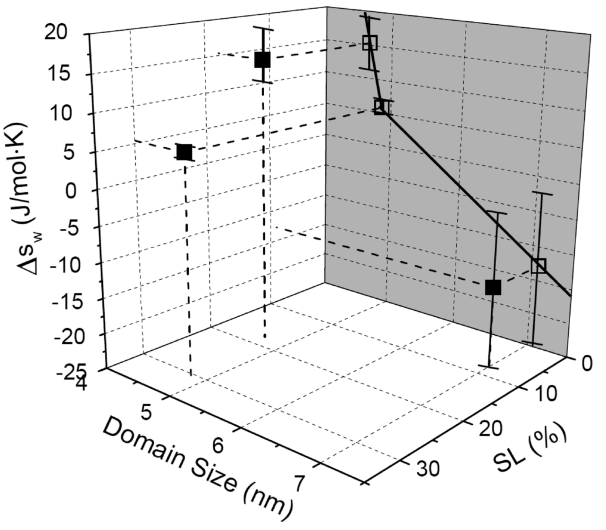

Figure 11. Partial molar entropy change at the order−disorder transition, Δs_w, as a function of SL and d. The error bars correspond to a confidence interval of 80%. The data point at SL = 31% and d = 5 nm was taken from our recent publication.[18] The plot indicates that the Δs_w is positive when the domain size is smaller than 6 ± 1 nm. The projection of data on the $\Delta s_w - d$ plane suggests that Δs_w decreases with increasing d.

In Figure 11 we plot Δs_w as a function of d, the domain size of the dry polymers at 20 °C, and SL. The magnitude and sign of Δs_w appear to depend on both of these parameters. Positive values of Δs_w are obtained in small channels at high SLs. An understanding of the microscopic underpinnings of Δs_w is required to decouple the effects of d and SL and to understand why Δs_w is positive in some systems. One possible scenario is that positive Δs_w values are obtained because the dissociation of SO_3^- counterions occurs more readily in the ordered state relative to the disordered state. In this case we expect SL to have a dominant effect on Δs_w. On the other hand, if water molecules themselves have more entropy in the ordered state due to lack of interruptions of the hydrogen-bonded network, then we expect d to also play a role in determining Δs_w. The projection of the limited data thus obtained on the $\Delta s_w - d$ plane (Figure 11) suggests that Δs_w decreases with increasing d (confidence interval is 80%). Further work is needed to substantiate this suggestion.

Conclusion

Humidity-induced phase transitions in poly(styrenesulfonate−methylbutylene) (PSS−PMB) block copolymers were accessed by varying sulfonation levels and molecular weights of copolymers. PSS−PMB samples with 5 nm domain spacing exhibited a disorder-to-order transition with increasing temperature at fixed relative humidity, while the PSS−PMB samples with 7 nm domain spacing exhibited an order-to-disorder transition with increasing temperature at fixed relative humidity. These phase transitions have a relatively small effect on the water uptake characteristics of the copolymers. Analysis of the data suggests

that the disorder-to-order transition is driven by an increase in the partial molar entropy of the water molecules, while the order-to-disorder transition is driven by more familiar driving forces wherein entropic contributions stabilize the disordered phase.

It is important to distinguish the present study from the vast body of previous literature on mixtures of block copolymers and selective solvents (e.g., refs 35−37). Most of these studies are restricted to uncharged systems, and all of the measurements were performed on closed systems where the solvent concentration in the polymer was fixed. In contrast, our study concerns an open system containing charged block polymers wherein the water concentration in the copolymer is governed by chemical equilibrium. If the fundamental thermodynamic relationship for the system is known, then data obtained from closed systems can readily be used to predict the properties of open systems (and vice versa).[38] In the absence of knowledge of the fundamental relationship, however, data obtained from open systems provide unique insight into the underpinnings of the observed phenomena. For example, the phase diagrams shown in Figure 6 can readily be obtained from experiments on closed systems. It would, however, not be possible to elucidate the role of the partial molar entropy of the solvent molecules from such experiments. We hope that the present work provides motivation for further studies on open block copolymer/solvent mixtures.

Acknowledgment. Major funding for this work was provided through the Electron Microscopy of Soft Matter Program at Lawrence Berkeley National Laboratory (LBNL) supported by the Director, Office of Science, Office of Basic Energy Sciences, Materials Sciences and Engineering Division, of the U.S. Department of Energy under Contract DE-AC02-05CH11231. The SANS facilities at NIST are supported in part by the National Science Foundation under Agreement DMR-0454672.[39] We thank Arup Chakraborty, Glenn Fredrickson, and Scott Milner for educational discussions.

References and Notes

(1) Huggins, M. L. *J. Chem. Phys.* **1941**, *9*, 440.
(2) Flory, P. J. *J. Chem. Phys.* **1941**, *9*, 660.
(3) The Flory−Huggins theory, originally developed for polymer/solvent systems, was extended to polymer blends and other multicomponent mixtures by: Scott, R. L. *J. Polym. Sci.* **1952**, *9*, 423.
(4) Fredrickson, G. H.; Helfand, E. *J. Chem. Phys.* **1987**, *87*, 697.
(5) de Genes, P.-G. In *Scaling Concepts in Polymer Physics*; Cornell University Press: Ithaca, NY, 1979.
(6) Leibler, L. *Macromolecules* **1980**, *13*, 1602.
(7) Helfand, E. *J. Chem. Phys.* **1975**, *62*, 999.
(8) Doi, M.; Edwards, S. F. In *The Theory of Polymer Dynamics*; Clarendon: Oxford, 1986.
(9) Leibler, L.; Benoit, H. *Polymer* **1981**, *22*, 195.
(10) Benoit, H.; Wu, W.; Benmouna, M.; Mozer, B.; Bauer, B.; Lapp, A. *Macromolecules* **1985**, *18*, 986.
(11) Broseta, D.; Fredrickson, G. H. *J. Chem. Phys.* **1990**, *93*, 2927.
(12) Ruegg, M. L.; Reynolds, B. J.; Lin, M. Y.; Lohse, D. J.; Balsara, N. P. *Macromolecules* **2006**, *39*, 1125.
(13) Flory, P. In *Principles of Polymer Chemistry*; Cornell University Press: Ithaca, NY, 1953; Chapter XIII.
(14) Balsara, N. P.; Eitouni, H. B. In *Thermodynamics of Polymer Blends, Physical Properties of Polymers Handbook*, 2nd ed.; Mark, J. E., Ed.; Springer: New York, 2007; Chapter 19, p 339.
(15) Nedoma, A. J.; Robertson, M. L.; Wanakule, N. S.; Balsara, N. P. *Macromolecules* **2008**, *41*, 5773.
(16) Han, C. C.; Bauer, B. J.; Clark, J. C.; Muroga, Y.; Matsushita, Y.; Okada, M.; Tran-Cong, Q.; Chang, T.; Sanchez, I. C. *Polymer* **1988**, *29*, 2002.
(17) Wang, Q.; Taniguchi, T.; Fredrickson, G. H. *J. Phys. Chem. B* **2004**, *108*, 6733.
(18) Park, M. J.; Nedoma, A.; Geissler, P. L.; Balsara, N. P.; Jackson, A.; Cookson, D. *Macromolecules* **2008**, *41*, 2271.
(19) Prausnitz, J. M.; Lichtenthaler, R. N.; Azevedo, E. G. In *Molecular Thermodynamics of Fluid-Phase Equilibria*, 3rd ed.; Prentice Hall: Upper Saddle River, NJ, 1999.
(20) Park, M. J.; Downing, K. H.; Jackson, A.; Gomez, E. D.; Minor, A. M.; Cookson, D.; Weber, A. Z.; Balsara, N. P. *Nano Lett.* **2007**, *7*, 3547.
(21) Park, M. J.; Balsara, N. P. *Macromolecules* **2008**, *41*, 3678.
(22) Park, M. J.; Kim, S.; Minor, A. M.; Hexemer, A.; Balsara, N. P. *Adv. Mater.* **2009**, *21*, 203.
(23) Adams, J. L.; Quiram, D. J.; Graessley, W. W.; Register, R. A.; Marchand, G. R. *Macromolecules* **1998**, *31*, 201.
(24) Beck Tan, N. C.; Liu, X.; Briber, R. M.; Peiffer, D. G. *Polymer* **1995**, *36*, 1969.
(25) Glinka, C. J.; Barker, J. G.; Hammouda, B.; Krueger, S.; Moyer, J. J.; Orts, W. J. *J. Appl. Crystallogr.* **1998**, *31*, 430.
(26) Kline, S. R. *J. Appl. Crystallogr.* **2006**, *39*, 895.
(27) Ehlich, D.; Takenaka, M.; Hashimoto, T. *Macromolecules* **1993**, *26*, 492.
(28) Ogawa, T.; Sakamoto, N.; Hashimoto, T. *Macromolecules* **1996**, *29*, 2113.
(29) Dai, H. J.; Balsara, N. P.; Garetz, B. A.; Newstein, M. C. *Phys. Rev. Lett.* **1996**, *77*, 3667.
(30) Bates, F. S.; Fredrickson, G. H. *Annu. Rev. Phys. Chem.* **1990**, *41*, 525.
(31) Matsen, M. W.; Bates, F. S. *Macromolecules* **1996**, *29*, 1091.
(32) Fredrickson, G. H.; Helfand, E. *J. Chem. Phys.* **1988**, *89*, 5890.
(33) Bates F. S.; Fredrickson, G. H. *Phys. Today* **1999**, *52*, 32.33.
(34) Almdal, K.; Rosedale, J. H.; Bates, F. S.; Wignall, G. D.; Fredrickson, G. H. *Phys. Rev. Lett.* **1990**, *65*, 112.
(35) Hanley, K. J.; Lodge, T. P.; Huang, C.-I. *Macromolecules* **2000**, *33*, 5918.
(36) Sakurai, S.; Hashimoto, T.; Fetters, L. J. *Macromolecules* **1996**, *29*, 740.
(37) Svensson, M.; Alexandridis, P.; Linse, P. *Macromolecules* **1999**, *32*, 637.
(38) Callen, H. B. In *Thermodynamics*; Wiley: New York, 1960.
(39) Certain commercial equipment, instruments, or materials (or suppliers, or software) are identified in this paper to foster understanding. Such identification does not imply recommendation or endorsement by the National Institute of Standards and Technology, nor does it imply that the materials or equipment identified are necessarily the best available for the purpose.